

Irreversible degradation of Nb₃Sn Rutherford cables due to transverse compressive stress at room temperature

Patrick Ebermann^{1,2} , Johannes Bernardi³, Jerome Fleiter¹, Friedrich Lackner¹, Florian Meuter¹, Magdalena Pieler³, Christian Scheuerlein¹ , Daniel Schoerling¹, Felix Wolf^{1,4}, Amalia Ballarino¹, Luca Bottura¹, Davide Tommasini¹, Frederic Savary¹ and Michael Eisterer² 

¹ European Organisation for Nuclear Research (CERN), Geneva, Switzerland

² Atominstitut (ATI), TU Wien, Vienna, Austria

³ University Service Centre for Transmission Electron Microscopy (USTEM), TU Wien, Vienna, Austria

⁴ Freiberg University of Mining and Technology, Freiberg, Germany

E-mail: friedrich.lackner@cern.ch

Received 30 January 2018, revised 5 March 2018

Accepted for publication 12 March 2018

Published 4 May 2018



Abstract

In the framework of the Future Circular Collider design study for a 100 TeV circular collider, 16 T superconducting bending magnets based on Nb₃Sn technology are being developed. A pre-stress on the conductor during magnet assembly at room temperature (RT) is needed to counteract the Lorentz forces during operation. The superconducting properties of the brittle Nb₃Sn superconductor are strain sensitive and excessive pre-stress leads to an irreversible degradation of the superconductor. In order to determine the level of acceptable pre-stress during the magnet assembly process, reacted and impregnated Nb₃Sn cables were exposed to increasing transverse compressive stress up to a maximum stress level of 200 MPa at RT. After each stress cycle, the critical current of the cable specimens were characterized at 4.3 K in the FRESCA cable test station. No significant critical current degradation was observed up to 150 MPa, followed by degradation less than 4% after a nominal stress of 175 MPa. A dramatic permanent critical current degradation occurred after applying a nominal stress of 200 MPa. A comprehensive post analysis consisting of non-destructive micro-tomography followed by microscopic characterization of metallographic cable cross sections was carried out after the critical current test to reveal cracks in the Nb₃Sn sub-elements of the loaded specimen.

Keywords: critical current, irreversible degradation, transverse compressive stress, Nb₃Sn, Rutherford cable, metallographic investigation of Nb₃Sn composite superconductors

(Some figures may appear in colour only in the online journal)

1. Introduction

Several aspects of manufacturing future accelerator magnets are being investigated by the Future Circular Collider (FCC) 16 T dipole programme [1]. One of the most critical topics is the irreversible electrical degradation due to the coil pre-stress applied during magnet assembly. The pre-stress on the coil is essential to counteract the Lorentz force during operation

minimizing movement of the conductor, which can cause a disturbance quench [2].

Considering that Nb₃Sn is a brittle material and that its superconducting properties are strain sensitive, the aim of this study is to determine the irreversible critical current degradation as a function of mechanical pre-stress, which is applied on reacted and impregnated Nb₃Sn coils for accelerator magnets at room temperature (RT).

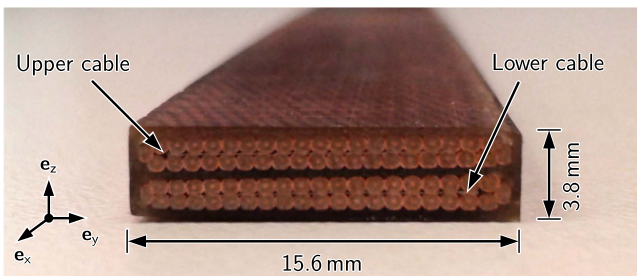


Figure 1. Cross section of the non-loaded part of two-stacked keystone Rutherford cable.

The superconductive behaviour of Nb_3Sn strands and cables during stress at cryogenic temperatures has already been investigated well [3–7]. The dominant load case in accelerator magnet coils is in transverse direction and its limit is roughly assumed to be at 150 MPa.

In the present study, transverse stress up to a nominal value of 200 MPa was applied in several stress steps to a Nb_3Sn Rutherford double cable stack at RT.

A dedicated facility was developed to this aim, with which transverse compressive stress can be applied. After each stress step, the cable stack was inserted in the sample holder of the FRESCA test station for I_c measurements [8].

Furthermore, a comprehensive post analysis was performed by x-ray micro computed tomography (micro-CT), followed by scanning electron microscopy (SEM) examination of metallographic cross sections of the 200 MPa loaded and non-loaded area of the cable sample. Samples from the identical cable stack were used for supplementary metallographic investigations.

2. Specimen and experimental details

The specimen was exposed to transverse stress at RT and subsequently transferred to the FRESCA test station for I_c measurements at cryogenic temperatures. This procedure was repeated after increasing the transverse stress stepwise until the critical current was drastically degraded.

2.1. Nb_3Sn Rutherford cable double stack specimen

A double stack of Nb_3Sn Rutherford cables was tested after reaction heat treatment and impregnation. The main parameters of the Nb_3Sn restacked-rod process (RRP) wire and the S-2 glass braiding insulated cable are summarized in tables 1 and 2, respectively [9].

A cross section of the cable double stack specimen can be seen in figure 1. The cross section dimensions of the specimen are $(15.6 \times 3.8) \text{ mm}^2$.

To use keystoned cables, which are also used for magnet coils and performing uniaxial stress on the surface the cables were arranged in a way to compensate the keystone. This achieves a planar surface of the sample for applying transverse stress.

As shown in the schematic of the entire specimen for the FRESCA test station (see figure 2), Nb-Ti current leads were

Table 1. Cable properties.

Manufacturer	CERN
Cable ID	HT15OC0190
Number of strands	40
Transposition pitch	100 mm
Keystone angle	0.79°
Mid-thickness	1.25 mm
Width	14.7 mm
Insulation	S-2 glass
Core	316 L
Packing factor	87.3%
Impregnation	CTD-101K

Table 2. Wire specification.

Manufacturer	Oxford Superconducting Technology (OST)
Wire type	RRP 144/169
Cu/non Cu ratio	1.08
Wire diameter	0.7 mm
Sub-element diameter	41 μm
Wire pitch length	14 mm
Virgin RRR	150
Virgin I_c (12 T, 4.3 K)	438 A
Heat treatment	48 h/210 °C 48 h/400 °C 50 h/650 °C

soldered on the top end of the cable sample with SnAg solder alloy to connect the specimen to the current supply. Furthermore, the two cables were soldered together at the bottom end to close the experimental circuit. This results in an anti-parallel current flow in the cable segment that was exposed to transverse stress. The cables were assembled with voltage tap pairs for recording voltage-current ($V-I$) characteristics and quench detection (see figure 2). The taps made of CuBe were placed directly on the entire width of the cable and bonded by diffusion at the reaction heat treatment. After the impregnation the lateral part of the taps were revealed and soldered with the signal wiring.

2.2. Set-up for applying transverse compressive stress

In order to apply well defined transverse stress on the cable stack, a tooling was designed to allow a homogenous pressure distribution and a precise measurement of the applied force. This tooling was integrated into a hydraulic press. For the entire set-up see figure 3. To avoid bending of the 1.73 m long cable specimen, it was placed on a support plate and further supports were added.

A uniform transverse pressure up to 230 MPa can be applied onto the 15.6 mm wide specimen using a 50 mm long stainless pressing tool. The load cells with a range from 0 to 200 kN and a measurement uncertainty of 0.05% were aligned to reach equally distributed load balancing on the four support points.

In addition to the force measurement with the load cells, pressure sensitive films from FujiFilm Corporation, so called

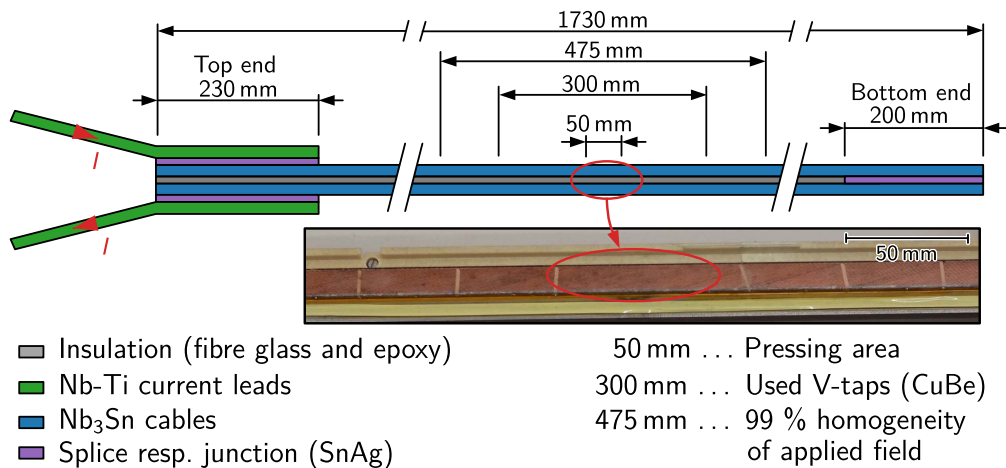


Figure 2. Schematic of entire FRESCA-compatible specimen with illustration of the pressing area.

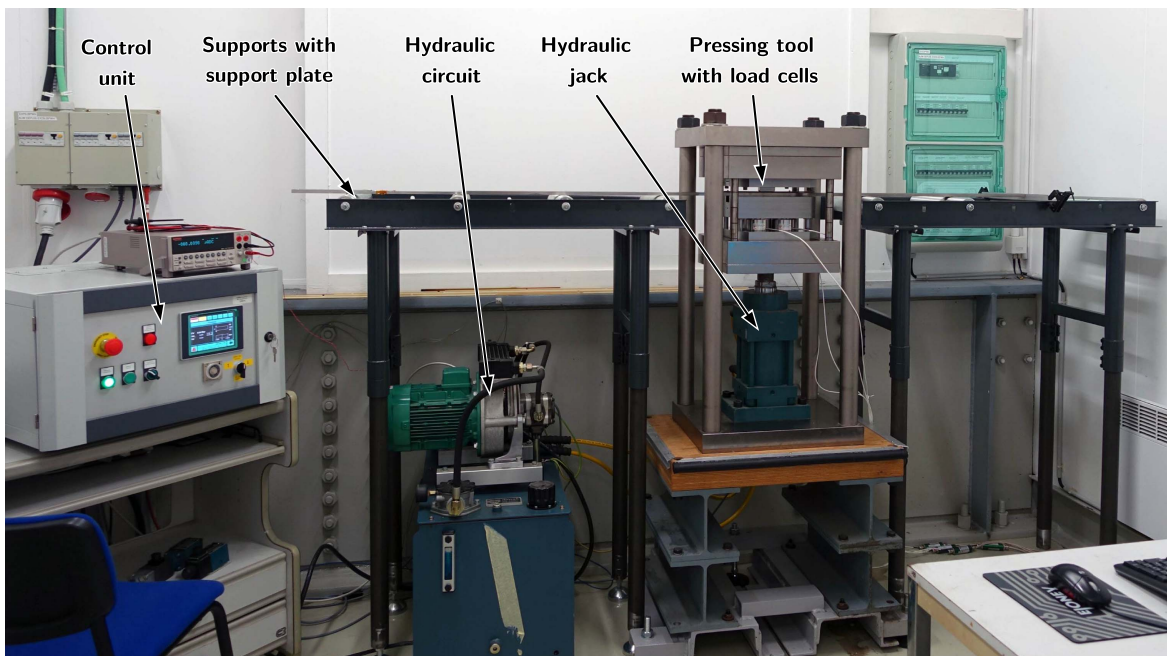


Figure 3. Set-up for applying transverse compressive stress on the double Rutherford cable stack.

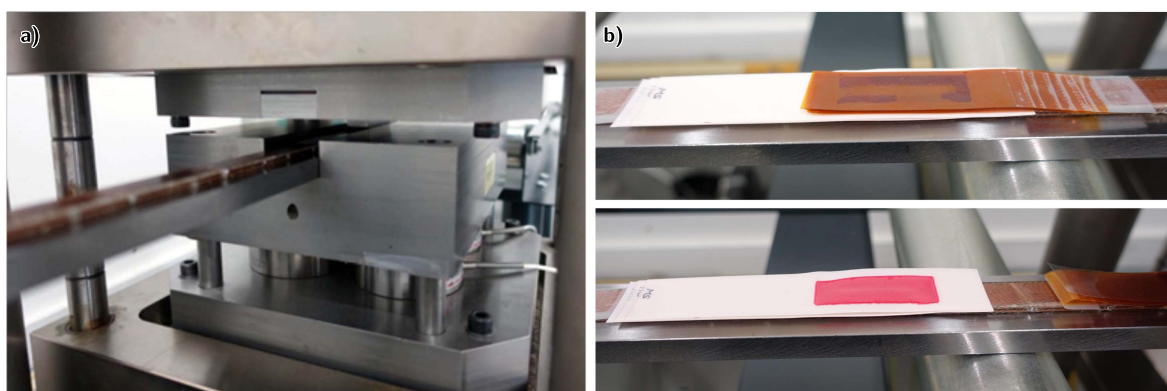


Figure 4. (a) Picture of the specimen in the pressing tool and (b) 1 mm thick polyimide foil stack intermediate layer with pressure sensitive films after applying a nominal stress of 175 MPa.

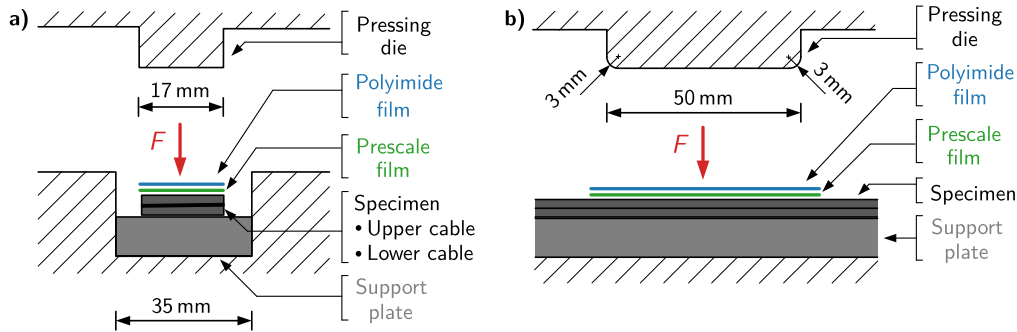


Figure 5. Schematic of pressing arrangement for applying transverse stress on the specimen (top view in (a) and side view in (b)).

Prescale films, were used [10]. This allowed analysing the pressure distribution on the surface of the specimen independently from the absolute force measured by the load cells. The Prescale films, which are available for several stress ranges, were placed between the cable sample and the pressing die and derived a two-dimensional colour density imprint of the pressurized area. The red colour density is nonlinearly related to the applied stress. For a quantitative analysis of the stress distribution measured by the Prescale film colour density distribution, a MATLAB script was developed and used to derive the pressure distribution. The integrated pressure distribution was compared with the force evaluated by the load cells. The proper interpretation is illustrated in a separate study (see [11]). To homogenize the pressure distribution on the specimen, the short edges of the pressing tool were rounded with a radius of 3 mm based on a FEM analysis, and foils of different materials (e.g. In, SnPb and SnAg foils) were tested as an intermediate layer. The best results were obtained with a 1 mm thick stack of polyimide foils, which was finally used [12]. The specimen during stress application can be seen in figure 4(a). The coloured imprint on the Prescale films underneath the polyimide layer after the stress application can be seen in figure 4(b).

For application of different transverse stress levels, the specimen was placed onto a support plate. The transverse pressure was transmitted via a pressing die with a length of 44 mm at RT (see figure 5). The stress was maintained constant for 2 min in order to reach a high reliability of pressure sensitive films as recommended in the manual [10].

2.3. Critical current measurements in the FRESCA test station

Irreversible damage of the Nb₃Sn cables caused by application of transverse compressive stress at RT was characterized by performing I_c measurements.

For this purpose the specimen was inserted into the FRESCA test station after each stress application [8]. This cable test facility allows tests up to a current of 32 kA in an applied field up to 9.6 T at 4.3 and 1.9 K. In the present study the critical current I_c was measured at a temperature of 4.3 K with the applied field ranging from 7 to 9.6 T. The resistive transition during the measurement was observed independently on both Nb₃Sn cables [13].

Direct current-current transformers were used to evaluate the current and a micro-voltmeter was used to measure the

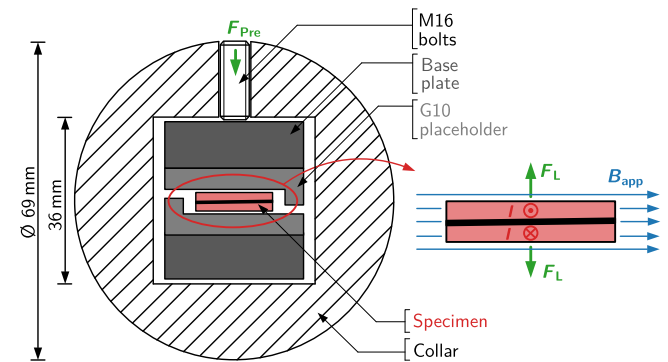


Figure 6. Mounting configuration during I_c measurement in the FRESCA cable test station as well as in left the applied field configuration and the resulting Lorentz force on the current-carrying specimen.

voltage drop across the voltage tap pairs. Additionally, a fast tracking data acquisition system was used for quench analysis.

The FRESCA dipole magnet was designed to ensure 99% field homogeneity along 475 mm. The specimen was placed in a sample holder surrounded by a collar and inserted through a 72 mm aperture into the inner cryostat. The pressing area of the specimen was entirely located in the 99% field homogeneity region and kept free of voltage taps to ensure an undisturbed surface.

In order to prevent disturbance quenches, the specimen was restrained with $F_{Pre} = 50$ MPa by the collar of the FRESCA sample holder generated by using M16 bolts every 40 mm, which is illustrated in figure 6. The applied stress decreases due to thermal contraction during cool down, which ensures the absence of reversible degradation [6].

The direction of the applied field B_{app} was always parallel to the large surface of the specimen and perpendicular to the current, which leads to a Lorentz force F_L configuration as described in figure 6. This corresponds to the field configuration with the highest peak field of the cable assembly. Current ramps of 100 A s⁻¹ and voltage tap pairs with a distance of 300 mm were chosen for measuring the V-I characteristics.

2.4. Metallographic preparation and SEM investigation of cable cross sections

Subsequent to the micro-CT analysis the same specimen was cut along preferred orientations and observed by SEM in

Table 3. Nominal stress, sum of the force measured with the load cells and average stress.

Nominal MPa	$F_{\text{LoadCells}}$ kN	$\sigma_{\text{LoadCells}}$ MPa	σ_{Prescale} MPa	$\Delta_{90\%}$ MPa	F_{Domain} kN	A_{Domain} %
50	33.0	48.0	—	—	—	—
100	68.9	100.4	—	—	—	—
125	85.2	124.2	—	—	—	—
150	103.0	150.1	142.4	[130.3, 154.5]	40.06	43.5
175	118.0	171.9	168.4	[142.2, 194.6]	105.0	73.1
200	137.9	200.9	194.1	[147.1, 241.1]	122.8	79.3

order to analyse the crack formation in the Nb₃Sn sub-elements. To ensure that the cracks were only induced by the transverse stress during the experiment, parts of the loaded and the non-loaded section of the specimen were inspected.

Two 25 mm wide samples from the loaded as well as from the non-loaded part of the specimen were cut with a diamond wire saw and embedded in epoxy resin. For each load case a metallographic sample of the ZY-plane (see figure 1), so called transverse cross section, and of the XY-plane (see figure 1), so called longitudinal cross section, were prepared.

The samples were grinded with fine-grained SiC grinding paper up to the target level. Afterwards the surface was polished with polishing papers in combination with water-based diamond paste as well as a vibratory polisher with colloidal silica. Finally the surface was automatically cleaned with a mixture of water rinsing and ultrasound followed by drying. For the SEM investigation the samples were priorly sputtered with Au/Pd.

The superconductive Nb₃Sn of the sub-elements is much harder than the surrounding Cu, so that removing Nb₃Sn particles tend to fill the wanted cracks or deposit on the Cu matrix. This blurring effect could be suppressed by optimizing the polishing and cleaning process. The wanted cracks presented also cavities on the metallographic prepared surface, which deposited liquids of the cleaning process. It appears after reducing the pressure in the SEM sample chamber and led to disturbances on the observed area, which could mainly prevent by using filter paper.

3. Results

3.1. Stress applied at RT

Table 3 compares the nominal (targeted) stress values with the stress determined with the direct force measurements using the load cells and the nominal pressing area of (44 × 15.6) mm², which is denoted as the average stress, $\sigma_{\text{LoadCells}}$. The pressure distribution on the surface of the specimen after exposure to nominal stress of 150, 175 and 200 MPa can be seen in figure 7. The white areas are points outside of the range of the Prescale films function provided in the manual, i.e. either too high or too low for the film used. Some stress peaks could be observed, which are probably caused by the surface roughness of the impregnated

specimen. The average stress σ_{Prescale} including the effectively used area A_{Domain} , i.e. pixels with stress magnitudes within the range of the used Prescale films, are also listed in table 3. The interval within 90% of the data that spreads around the average stress is also listed in table 3. The reliability of σ_{Prescale} depends strongly of the relative number of pixels, which hold a stress value within the range of the Prescale film as indicated by F_{Domain} and A_{Domain} .

Optical inspections after every pressure application yields epoxy cracks after the 150 MPa step on both sides. They could not be correlated with the cable surface such as the transposition pitch direction and were influenced additionally by the thermal cycling.

3.2. Critical current after different transverse compressive stress levels applied at RT

The recorded $V(I)$ curves at the highest applied field of 9.6 T of all pressure steps are plotted in figure 8, for the obtained data see table 4.

To prevent extrapolation uncertainties, the electrical field criterion $I_c = I(E = E_c)$ was reduced from the recommended $E_c = 10 \mu\text{V m}^{-1}$ to $E_c = 3 \mu\text{V m}^{-1}$ to ensure that measurement points are available at the I_c determination point [14]. For evaluating I_c , the corrected $V-I$ characteristics were calculated, i.e. the parasitic induction offset voltage and the resistive part of the virgin measurement was reassessed. Due to the low number of measurement points in the resistive transition the analysis of the n -value, according to the IEC61788-2 standard [14], was equivocal and not representative. In addition, the dependency of the upper critical field $B_{c2}(4.3 \text{ K})$ on the transverse stress was not clearly determinable by using the Kramer extrapolation due to relative low limitation of the applied field to 9.6 T compared to $B_{c2}(4.3 \text{ K})$ of Nb₃Sn composite superconductors.

The completed critical current results I_c (markers) as a function of the peak field $B_{\text{Peak}}(I)$ are shown in figure 9 including the scaling law trend curves (lines) derived by Kramer ($I_c = C b^{-\frac{1}{2}}(1 - b)^2$) with $b = B/B_{c2}$ and C and B_{c2} as fitting parameters [4]. The magnetic peak field $B_{\text{Peak}}(I) = \max(B) = \max[B_{\text{app}} + B_{\text{self}}(I)]$ was composed of the superposition of the applied homogeneous field B_{app} and the maximal self-induced field $B_{\text{self}}(I) = k_I I$ where $k_I = 80 \text{ mT kA}^{-1}$ computed with a FEM model. Due to the anti-parallel current flow, the peak field was located on the strands in the centre of the specimen, which means that

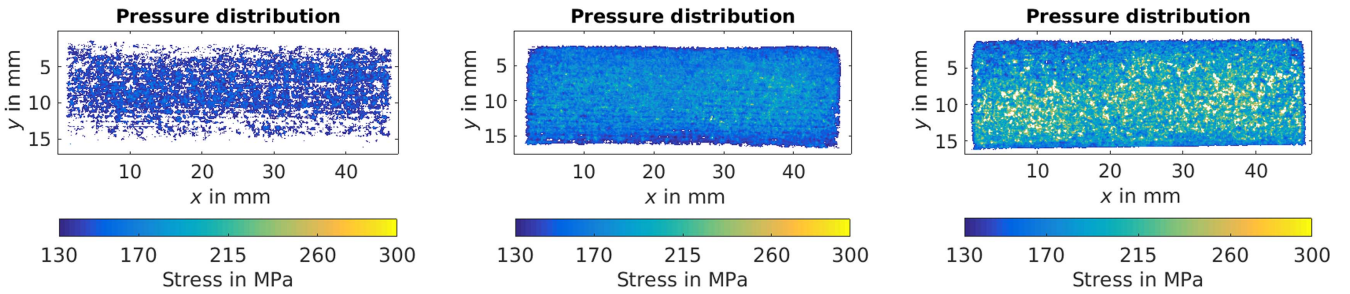


Figure 7. Analysis of the Prescale films of type HHS (i.e. evaluation range of 130–300 MPa) after the 150 MPa (left), 175 MPa (middle) and 200 MPa cycle (right).

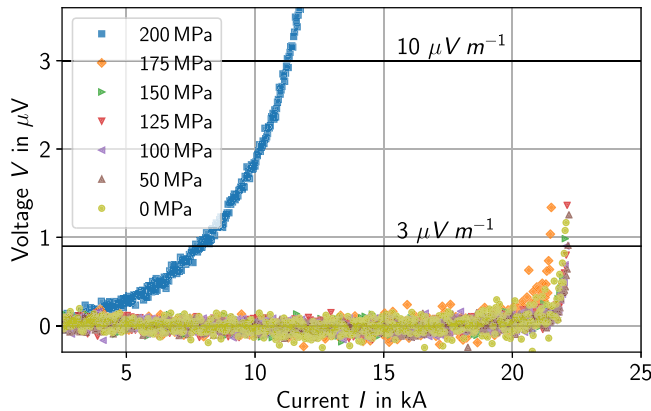


Figure 8. Comparison of corrected V - I characteristics of the upper cable at $\max(B_{app}) = 9.6$ T and $T = 4.3$ K after the application of different transverse compressive stress levels.

Table 4. Critical current at $\max(B_{app}) = 9.6$ T and $T = 4.3$ K measured after application of different stress levels at RT.

σ_{nominal} MPa	I_c kA	$I_c/I_{c,0\text{MPa}}$ (-)
0	22.06	1.00
50	22.23	1.01
100	22.20	1.01
125	22.16	1.00
150	22.15	1.00
175	21.45	0.97
200	7.90	0.36

the earliest expected quench occurred in the centre of the specimen.

The specimen showed the same degradation behaviour at all applied fields. Up to 150 MPa no degradation was detected. A small degradation (3%) could be quantified after applying 175 MPa. After a nominal load of 200 MPa, the specimen showed a strong degradation (64%).

Considering that the two measured cables were quenching independently, the results of the lower cable were analysed too [13]. It showed the same behaviour as the upper cable described. For comparison, the I_c degradation of the upper and the lower cable at the maximum applied field is plotted in figure 10. After the last pressure steps the two

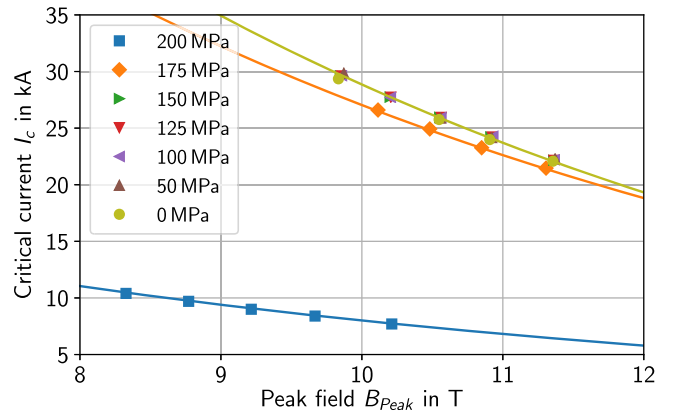


Figure 9. Critical current of the upper cable at $T = 4.3$ K as a function of the peak field after each pressure level.

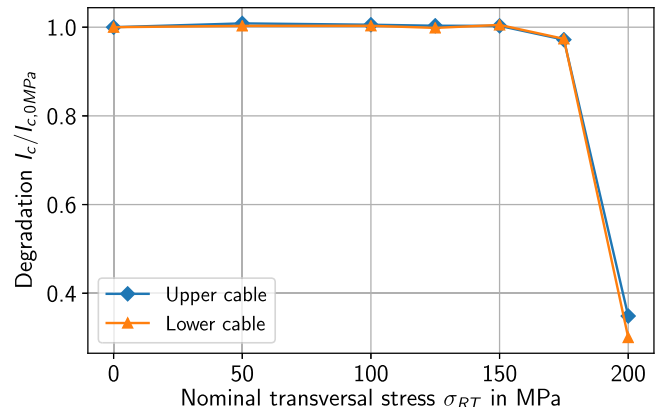


Figure 10. Comparison of the relative critical current degradation of the upper and lower cable as a function of the applied transverse stress at RT measured at $B_{app} = 9.6$ T and $T = 4.3$ K.

cables differ, which can be tracked down to the necessary low electrical field criterion and a marginal different n -value.

3.3. X-ray computed tomography of the Nb_3Sn Rutherford cable double stack specimen

After the completion of the I_c measurements up to a nominal stress of 200 MPa, a post analysis of the cable double stack by non-destructive micro-CT was performed in order to verify

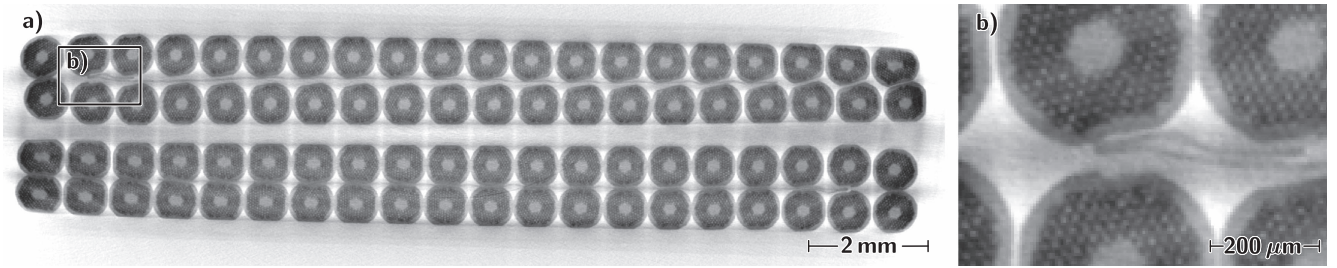


Figure 11. Micro-CT cross section of the 200 MPa loaded Nb₃Sn Rutherford double cable stack (a) including a detailed view of the strands (b) and the steel core at thick cable edge.

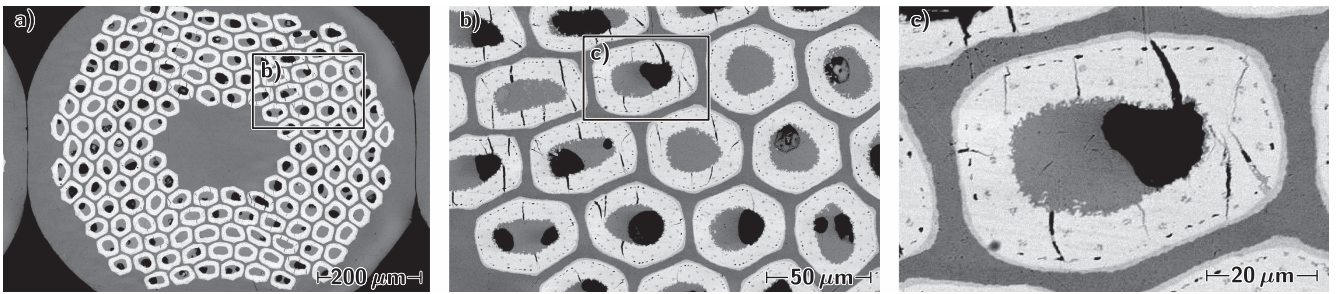


Figure 12. SEM micrographs of transverse metallographic cross section of the 200 MPa loaded area of the upper cable centre.

permanent deformation caused by the iterative stress applications.

The micro-CT was performed using a laboratory scanner with a 225 kV micro focus x-ray tube with 6 μm focal spot size and a flat panel detector with $2^{11} \times 2^{11}$ pixels [15]. The spatial resolution of the micro-CT scans is 10 μm. Thus, the spatial resolution of the micro-CT was not sufficient for detecting the investigated cracks in Nb₃Sn sub-elements of the cables. A micro-CT cross section of the specimen after application of a transverse stress of 200 MPa is shown in figure 11(a). The severe strand deformation on the cables edges caused by the cabling process is clearly visible, which is additional magnified in figure 11(b) [16].

Deformations and cracks in the impregnation cannot be visualized by x-ray tomography, due to the weak x-ray absorption in the CTD-101K epoxy. Permanent cable deformation caused by the experiment was smaller than the spatial resolution of the micro-CT experiment. The transversal microscopy revealed cracks with a typical width between 1 and 3 μm, which is below the spatial resolution. A comparison of the pressed area with an arbitrarily non-compressed area to identify the cable deformation was not representative, due to the manufacturing accuracy e.g. cabling and impregnation.

3.4. Metallographic examination of a non-loaded and the 200 MPa loaded part of the specimen

The SEM images of the cross section of the loaded sample revealed many cracks. The highest crack density could be observed in the centre part of the upper cable (upper row of strands). A typical strand from this area can be seen in figure 12 including magnified characteristic extractions in the

additional sub-figures. A micrograph of a similar position of the non-loaded sample is shown in figure 13, where no cracks could be found.

Strands from the loaded area showed a characteristic spatial crack distribution in the transverse cross section, which can be seen in figure 12(a). This pattern helps estimating in which depth of the longitudinal cross section the sample has to be prepared for efficient crack investigation. Figure 12(c) shows a cracked sub-element in detail. The cracks tend to be parallel to the applied transverse stress and extend from the inner residual α-bronze to the Nb diffusion barrier. Voids inside the sub-elements are not artefacts of the metallographic preparation and are produced during reaction heat treatment [17]. In the observed area voids tend to act as stress concentrators that induce larger cracks.

In a following step the longitudinal cross sections were prepared to identify the shape of the above described cracks in longitudinal surface. Therefore, the upper row of strands (upper cable) was examined. About one third of the row was removed planarly by metallographic preparation. An overview of the loaded sample is provided in figure 14(a), which displays a part of the longitudinal cross section of a damaged strand. Long as well as short cracks could be observed and a preferred propagation direction in longitudinal direction could be identified, i.e. longitudinal cracks.

In contrast to the transverse stress performed in this experiment, bending stress caused mainly cracks perpendicular to the transport current direction, i.e. transversal cracks as preceding bending tests published by Jewell *et al* showed (see [18]). Figure 15 presents the non-loaded part, where no cracks could be found.

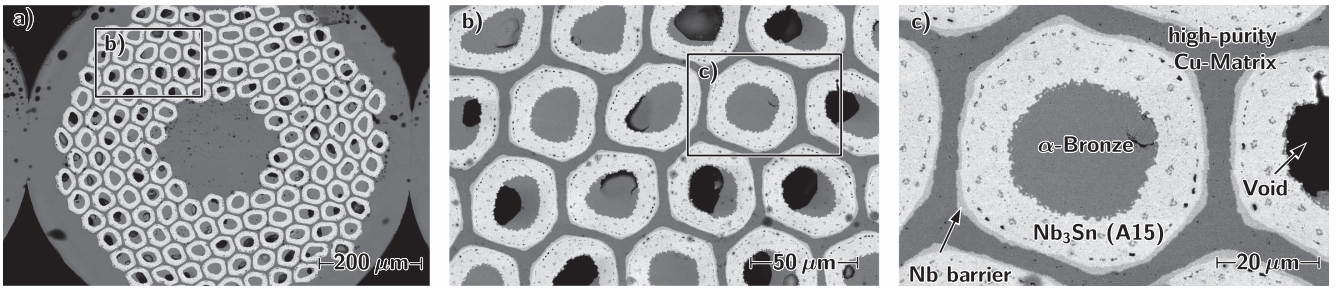


Figure 13. SEM micrographs of transverse metallographic cross section of an unloaded area of the upper cable centre.

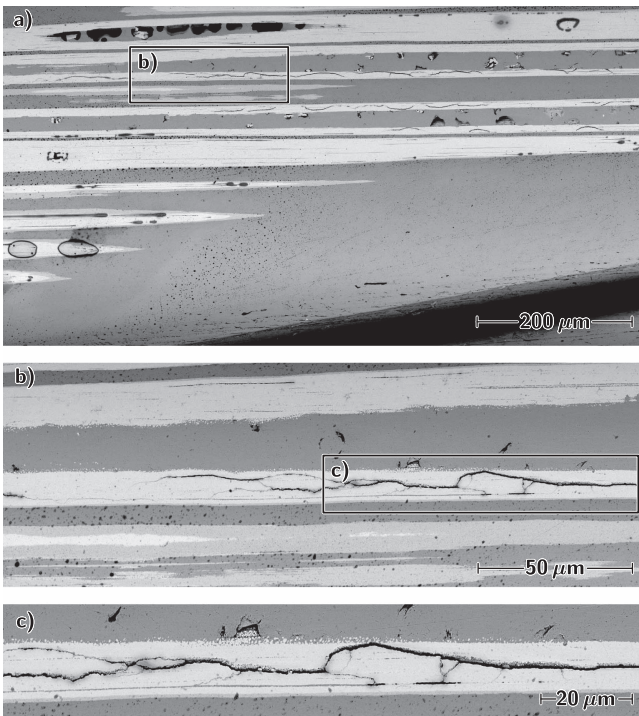


Figure 14. SEM micrographs of longitudinal metallographic cross section of the 200 MPa loaded area of the upper cable centre.

3.5. Metallographic examination of 150 MPa, 175 MPa and 200 MPa loaded samples

The 1.73 m long specimen, which was measured with the FRESCA cable test station, was cut into several parts for further investigation. Parts without any voltage taps and heaters were loaded according to the same procedure as described in sections 2.3 and 3.1 to certain stress levels to complement the above presented results.

The stressed samples were metallographically prepared with the same procedure as the samples described in section 3.4 and investigated with an optical microscope (OM). No cracks could be observed in samples loaded with less than 175 MPa. Figure 16 shows a comparison of the centre part of the upper cable (upper row of strands) after the stress levels of 150, 175 and 200 MPa. Sub-elements of the 150 MPa case (figures 16(a) and (d)) are undamaged. The 175 MPa case (figures 16(c) and (f)) can be considered as the starting level of crack initiation followed by the 200 MPa case (figures 16(b) and (e)) with clearly ruptured sub-elements.

Thus, the observed crack initiation after a certain stress supports the results of the I_c measurements presented in section 3.2.

4. Discussion

For the tested specimen made of RRP wires a transverse compressive stress of 150 MPa applied at RT did not cause degradation of the critical current within the experimental accuracy, which confirms the common limitation of 150 MPa with an additional margin, considering the degradation less than 4% after the 175 MPa load step. After applying 200 MPa pressure the critical current of the sample was heavily degraded and this load case is not recommendable for magnet production.

To deliver application-oriented results for magnet manufacturing technology, reacted and impregnated Rutherford cables instead of a single wire were chosen to include also the material and geometry effects of the insulation and the cable in the stress application. However, the high requirements of cable tests with currents above 20 kA restricted the investigation, so that only the critical current could be used unequivocally for characterization.

For interpretation of the provided data it must be considered that the mechanical properties of Nb₃Sn composite compounds at RT and cryogenic temperature differ. Hence, the performance loss of Nb₃Sn cables caused by stress at RT differs from the performance loss caused by stress at cryogenic temperatures.

Nevertheless, it must be mentioned that the optimized and measured homogenous stress on the surface, which is also the aim for the collaring of the magnets gives only an indirect statement about the intrinsic stress threshold on the superconductive sub-element. The latter is finally responsible for the observed cracks and the investigated and crucial performance loss. The mechanical properties of the relatively soft epoxy, the annealed Cu stabilizer as well the cable geometries influence mainly the relationship between the performed and measured stress distribution on the surface and the stress on the sub-elements. Considering that the peak field during I_c measurements is located in the middle of the specimen, the irreversible influence of stress on the centred strands is crucial, depending on the level of irreversible degradation of the specimen.

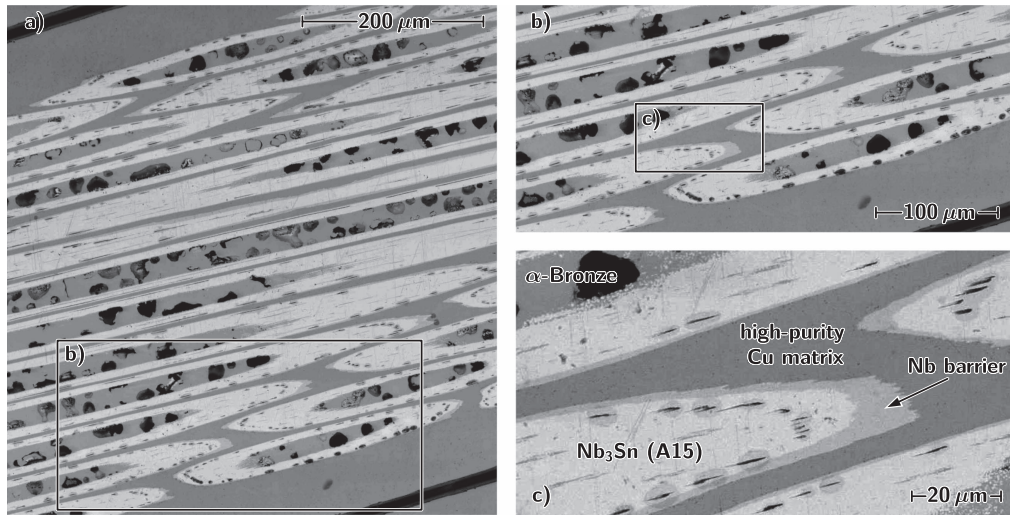


Figure 15. SEM micrographs of longitudinal metallographic cross section of a non-loaded area of the upper cable centre.

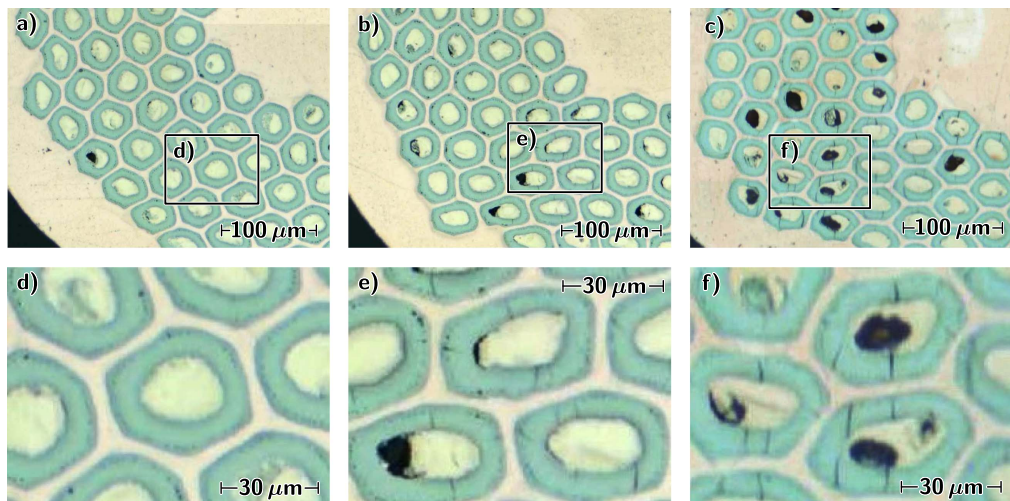


Figure 16. OM micrographs of transverse metallographic cross section of a 150 MPa (a), (d), 175 MPa (b), (e) and 200 MPa (c), (f) loaded area from the centre of the upper cable.

A strain caused degradation effect due to residual stress caused by the expectable plastic deformation of the soft Cu matrix beneath the crack initiation level of 175 MPa could not be clarified unequivocally on basis of the presented results.

The metallographic investigations revealed cracks in the superconductive sub-elements as well as their spatial distribution within the specimen, which are assumed to be the reason of I_c degradation according to results in section 3.5. The transverse cross section shows information about the crack distribution, which gave also an estimation of the stress distribution within the cable and strand during applied transverse stress at RT. According to the observations of the longitudinal cross section the typical shape of the cracks in sub-elements could be identified, which are mostly longitudinal cracks. They differ from cracks generated by bending or tensile stress, which cause transversal cracks in sub-elements [18]. In the observed areas (e.g. figure 14) the longitudinal shape of the cracks creates in the most cases a shrinkage of the effective superconductive cross section and

not an entire interruption of the superconductive material in transport current direction, which could be observed after bending stress (e.g. [18]).

5. Conclusion

The effect of transverse compressive stress applied at RT on the critical current of a reacted and impregnated Nb₃Sn Rutherford cable stack has been measured.

No critical current degradation was detectable after a nominal stress of up to 150 MPa. An irreversible critical current degradation of less than 4% at 4.3 K and an applied field of 9.6 T was observed after applying a nominal stress of 175 MPa at RT. After loading to 200 MPa the critical current is strongly degraded.

The metallographic examination of the 200 MPa loaded cable stack reveals cracks and their characteristic longitudinal shape in the Nb₃Sn sub-elements as well as their spatial

distribution within the specimen in the transverse cross sections. Additionally metallographic examinations of initially identical cable stacks show that the investigated crack initiation starts to occur at transverse stress of about 175 MPa, which corresponds to the measured I_c degradation.

Acknowledgments

We would like to thank the team of the Large Magnet Facility (CERN-TE-MSC-LMF). Special thanks go to O Kalouguine and G Peiro from the FRESCA team for support during handling the sample as well as performing the I_c measurements. Warm thanks to D Meinel from the Federal Institute for Material Research and Testing (BAM), Berlin, Germany for the valuable micro-CT measurement. Also thanks to J Gruber from the USTEM, Vienna, Austria as well as A Gallifa Terricabras and J Busom Descarrega (CERN-EN-MME-MM) for the careful preparation of the metallographic samples. This work was supported by the FCC 16 T programme and carried out by the workgroup wound conductor test facilities.

ORCID iDs

Patrick Ebermann  <https://orcid.org/0000-0002-9792-9275>
 Christian Scheuerlein  <https://orcid.org/0000-0002-8512-7187>
 Michael Eisterer  <https://orcid.org/0000-0002-7160-7331>

References

- [1] Tommassini D *et al* 2017 Status of the 16 T dipole development program for a Future Hadron Collider *IEEE Trans. Appl. Supercond.* **28** 4001305
- [2] Russenschuck S 2010 *Field Computation for Accelerator Magnets* (Weinheim: Wiley-VCH) (<https://doi.org/10.1002/9783527635467>)
- [3] Ekin J W 1987 Effect of transverse compressive stress on the critical current and upper critical field of Nb₃Sn *J. Appl. Phys.* **62** 4829
- [4] Ekin J W 2010 Unified scaling law for flux pinning in practical superconductors: I. Separability postulate, raw scaling data and parameterization at moderate strains *Supercond. Sci. Technol.* **23** 083001
- [5] Ten Kate H, Weijers H W and von Oort J M 1993 Critical current degradation in Nb₃Sn cables under transverse pressure *IEEE Trans. Appl. Supercond.* **3** 1334–7
- [6] Bordini B, Alknes P, Ballarino A, Bottura L and Oberli L 2014 Critical current measurements of high- J_c Nb₃Sn Rutherford cables under transverse compression *IEEE Trans. Appl. Supercond.* **24** 9501005
- [7] Jacob B, Pasztor G, Bona M and Asner A 1991 Reduced sensitivity of Nb₃Sn epoxy-impregnated cable to transverse stress *Cryogenics* **31** 390–1
- [8] Verweij A P, Genest J, Knezovic A, Leroy D F, Marzolf J-P and Oberli L R 1999 1.9 K test facility for the reception of the superconducting cables for the LHC *IEEE Trans. Appl. Supercond.* **9** 153–6
- [9] Bordini B, Ballarino A, Oberli L and Richter D 2016 CERN conductor and cable development for the 11 T dipole *HL-LHC Collaboration Meeting on DS 11 T Dipole Grounds (CERN, Geneva, Switzerland)*
- [10] FujiFilm Corporation 2018 Prescale pressure measurement film www.fujifilm.com/products/prescale/
- [11] Ebermann P and Wolf F 2017 Evaluation script for analysing pressure measurement films with office scanners *Technical Report EDMS- 1885552* (Geneva: CERN)
- [12] Wolf F, Ebermann P, Lackner F, Mosbach D, Scheuerlein C, Schladitz K and Schoerling D 2017 Characterization of the stress distribution on Nb₃Sn Rutherford cables under transverse compression *IEEE Trans. Appl. Supercond.* **28** 8400106
- [13] Fleiter J, Bordini B, Ballarino A, Oberli L, Izquierdo S and Bottura L 2015 Quench propagation in Nb₃Sn Rutherford cables *IEEE Trans. Appl. Supercond.* **25** 4802504
- [14] IEC 61788-2 2006 *Superconductivity Part 2: Critical Current Measurements, DC Critical Current of Nb₃Sn Composite Superconductors* (IEC Standard)
- [15] Kelly U, Richter S, Redenbach C, Schladitz K, Scheuerlein C, Wolf F, Ebermann P, Lackner F, Schoerling D and Meinel D Nb₃Sn wire shape and cross sectional area inhomogeneity in Rutherford cables *IEEE Trans. Appl. Supercond.* **28** 4800705
- [16] Fleiter J, Ballarino A, Bonasia A, Bordini B and Richter D 2017 Optimization of Nb₃Sn Rutherford cables geometry for the high-luminosity LHC *IEEE Trans. Appl. Supercond.* **27** 4004305
- [17] Scheuerlein C, Michiel M D and Buta F 2009 Synchrotron radiation techniques for the characterisation of Nb₃Sn superconductors *IEEE Trans. Appl. Supercond.* **19** 2653–6
- [18] Jewell M C, Lee P J and Larbalestier D C 2003 The influence of Nb₃Sn strand geometry on filament breakage and bend strain as revealed by metallography *Supercond. Sci. Technol.* **16** 1005